JOURNAL OF GEOPHYSICAL RESEARCH, VOL. 100, NO. A2, PAGES 1811–1822, FEBRUARY 1, 1995

Study of dust in the vicinity of Dione using the Voyager 1 plasma wave instrument

D. Tsintikidis, W. S. Kurth, and D. A. Gurnett
Department of Physics and Astronomy, University of Iowa, Iowa City

D. D. Barbosa
Institute of Geophysics and Planctary Physics, University of California, Los Angeles

Abstract. The flyby of Voyager 1 at Saturn yielded the detection of a large variety of plasma waves, for example, chorus, hiss, and electron cyclotron harmonics. Just before the outbound equator crossing, the Voyager 1 plasma wave instrument detected a strong, well-defined low-frequency enhancement in signal levels. Initially, it was thought that this enhancement was due to plasma waves, but more recently it was suggested that dust impacts might be at least partial contributors. In this report we present evidence that dust impacts are partly responsible for the low-frequency enhancement. A new method of analysis which relies mainly on the 16-channel spectrum analyzer has been used to derive the dust impact rate. The available wideband waveform observations (which have been used previously to study dust impacts) were useful for calibrating the impact rate from the spectrum analyzer data. The mass and hence size of the dust particles were also obtained by analyzing the response of the plasma wave spectrum analyzer. The results show that the region sampled by Voyager 1 is populated by dust particles that have rms masses of up to few times 10^{-11} g and sizes of up to a few microns. The dust particle number density is of the order of 10^{-3} m^{-3}. The optical depth of the region sampled by the spacecraft is approximately 10^{-6}. The particle population is centered at 2470(±150) km south of the equatorial plane and has a north-south FWHM (full-width, half-maximum) thickness of 4130(±450) km. The dust may be part of the *E* ring or a localized ringlet associated with Dione.

1. Introduction

The dust environment of Saturn has been studied extensively. A great deal of knowledge has resulted from the direct detection of dust, that is, from the micrometeoroid bombardment detectors ("beer can" experiment) onboard Pioneer 11 [*Humes*, 1980], and from the plasma wave and planetary radio astronomy instruments onboard Voyager 2 [*Scarf et al.*, 1982; *Warwick et al.*, 1982]. The dust dynamics have also been (and are still being) studied using analytical and numerical techniques [e.g., *Xu and Houpis*, 1985; *Burns and Schaffer*, 1989; *Horanyi et al.*, 1992; *Hamilton*, 1993]. The Voyager 2 plasma wave instrument detected intense, impulsive noise at each of the three outer planets (Saturn, Uranus, Neptune) that has been attributed to micron-sized dust particles hitting the spacecraft body [*Gurnett et al.*, 1983, 1987, 1991; *Aubier et al.*, 1983; *Pedersen et al.*, 1991; *Tsintikidis et al.*, 1994]. As a particle hits the spacecraft at a relative velocity of a few tens of kilometers per second, it is vaporized and heated to a high temperature. The high temperature produces a small, partially ionized cloud of gas which expands rapidly outward from the impact site. Part of the charge in the cloud is collected by the electric antennas onboard the spacecraft. The mass and the size of the particles can be estimated by analyzing the amplitude of the voltage pulse recorded by the low-resolution 16-channel plasma wave spectrum analyzer. Also, the high-resolution wideband waveform receiver data can be used to calculate the impact rate. When the impact rate is combined with the spacecraft cross-sectional area and the relative velocity between the spacecraft and the dust particles, the particle number density can also be calculated. All of these factors combine to produce a general picture of the dust environment sampled by the spacecraft [e.g., *Gurnett et al.*, 1991, Figure 13].

The analysis of the dust environment near the *G* ring by Voyager 2 was greatly aided by the availability of wideband data recorded within and on either side of the dust ring. Subsequent analysis of dust at Uranus and Neptune also relied heavily on the wideband data. However, during the Voyager 1 flyby of Saturn, relatively few wideband frames were recorded, and most of these were located well away from the equatorial plane. Hence it was not possible to derive a rate profile (and consequently the number density profile) similar to that obtained by Voyager 2 [see *Tsintikidis et al.*, 1994]. To overcome this deficiency, we have developed a new method of determining the impact rates by using the 16-channel spectrum analyzer data and the relatively few high resolution data frames that are available.

In this paper we present a detailed study of the low-resolution data recorded by the plasma wave instrument onboard Voyager 1 around the time of closest approach to Saturn. We give (1) a detailed description of the data used in

Copyright 1995 by the American Geophysical Union.

Paper number 94JA02357.
0148-0227/95/94JA-02357$05.00

the study, (2) a thorough description of the method used to derive our results, (3) an interpretation of the data in terms of number density, mass, and sizes of the dust particles, (4) a validation of our results compared with theoretical predictions and results from other independent photometric studies, and (5) a short discussion of the possible origin of the particles.

2. Observations

A spectrogram of the plasma wave observations obtained by Voyager 1 at Saturn is given in Plate 3 of *Kurth and Gurnett* [1991]. Among the features that can be seen in this spectrogram is one tentatively labeled "dust impacts" centered around 0410 spacecraft event time (SCET) on November 13, 1980. At this time the spacecraft was outbound at approximately 6.1 R_S (1 R_S = 60,330 km), just below the equatorial plane. The feature looks similar to the intense, impulsive, dust-attributed noise that was observed during the other planetary encounters accomplished by Voyager 2 (see the dust signatures at Uranus and Neptune in Plates 4 and 5 of *Kurth and Gurnett* [1991]). The most definitive proof that dust exists in the area sampled by Voyager 2 comes from the waveform data. The signature of a dust impact consists of a single pulse followed by a recovery waveform that is unlike any other known plasma wave waveform [e.g., *Gurnett et al.*, 1983, Figures 3 and 5]. The waveform data can be used to determine particle impact rates and number densities by following the technique of *Gurnett et al.* [1987, 1991] or *Tsintikidis et al.* [1994]. However, no wideband waveform frames (high-resolution data) were available at the time that Voyager 1 crossed the equatorial plane of Saturn. Hence it was not clear if the feature was a result of plasma wave activity or dust impacts or both. *Barbosa and Kurth* [1993] interpreted the Voyager 1 plasma wave observations at Saturn's inner magnetosphere in terms of whistler mode and electrostatic electron cyclotron harmonic waves. On the basis of a theoretical analysis, these authors determined that the observed fluxes of superthermal electrons were sufficient to produce whistler mode waves and electron cyclotron harmonic waves through a loss cone instability. Furthermore, they concluded that a moderate anisotropy in the hot electron population existed in the equatorial region at L values ranging from 5 to 8. However, *Barbosa and Kurth* [1993] did not exclude the possibility that the noise in question may be caused by dust impacts. *Kurth and Gurnett* [1991] also suggested that the low-frequency enhancement, near the ring plane crossing, could be attributed to dust impacts. The purpose of the present study is to determine if dust impacts contribute to this enhancement and, if so, determine the characteristics of the dust population.

The antennas used by the Voyager plasma wave receiver are operated as an electric dipole, meaning that the plasma wave instrument (PWS) measures the potential difference between the two antenna elements. The signals from the antennas are processed in two ways. First, a 16-channel spectrum analyzer provides absolute measurements of the voltage spectral densities covering the range from 10 Hz to 56 kHz. There are four logarithmically spaced channels per decade. The spectrum analyzer has two logarithmic compressors. Each compressor consists of a detector whose output is proportional to the logarithm of the amplitude of the signal passing through the filter that is being sampled.

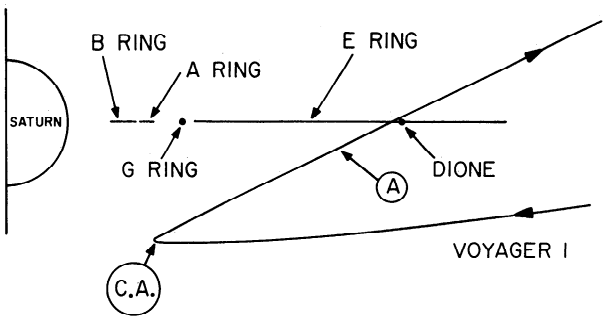

Figure 1. A perspective view of the Voyager 1 trajectory by Saturn. The spacecraft crossed the equatorial plane at 6.24 R_S (1 R_S = 60,330 km), very close to Dione's orbit (6.28 R_S). The angular separation between the spacecraft and Dione was about 38°. The radial extent of some of the rings is also shown. The circled A shows the position of the spacecraft when the last wideband data frame was taken before the equatorial plane crossing: 5.38 R_S radial distance and −4.53 degrees of latitude. The circled C.A. shows the closest approach position of the spacecraft: 3.05 R_S radial distance and −39.51° of latitude.

The 16-channel spectrum analyzer does not have peak detection. The channels are sampled sequentially until the full spectrum has been obtained. The lower and upper eight channels are processed separately by two logarithmic compressors. The two frequency ranges are stepped through nearly simultaneously. The filters have a bandwidth of ~±15% for the lowest eight frequencies and ~±7.5% for the highest eight frequencies. The time constant of the logarithmic compressor is about 50 ms for the lower eight channels and about 42 ms for the upper eight channels [*Kurth et al.*, 1983]. A full 16-channel spectral scan is completed once every 4 s. Second, a wideband receiver provides waveforms in a frequency band from 50 Hz to 12 kHz. The wideband data are obtained in 48-s-long "frames." Each frame contains 800 60-ms subsequences consisting of 4-bit measurements of the potential between the two antenna elements sampled at a rate of 28,800 s^{-1}. An automatic gain control (AGC) is used to maintain an almost constant output signal amplitude to provide a large dynamic range. The time constant of the AGC is 0.5 s. The PWS instruments onboard the two Voyager spacecraft are identical. For more details on the instrumentation, see *Scarf and Gurnett* [1977].

Figure 1 shows the Voyager 1 spacecraft trajectory. The spacecraft periapsis was at a radial distance of 3.05 R_S and a latitude of −39.51° on November 12, 1980. During the outbound trajectory it crossed the equatorial plane at 0418:30 SCET on November 13, 1980, at 6.24 R_S, just inside Dione's orbit, which is located at a radial distance of 6.28 R_S. At the time of the equatorial plane crossing the relative distance between the spacecraft, and Dione was about 250,000 km. Figure 2a shows all the channels of the 16-channel spectrum analyzer for a 4-hour period centered on the equator crossing. A relatively smooth increase and decrease in signal levels below a few kilohertz can be seen centered at approximately 0410 SCET. At the lowest frequencies a series of bursty signals can be observed. There are certain similarities between the measurements obtained at Saturn by the Voyager 1 PWS and those obtained at Saturn, Uranus, and Neptune by the Voyager 2 PWS [*Tsin-*

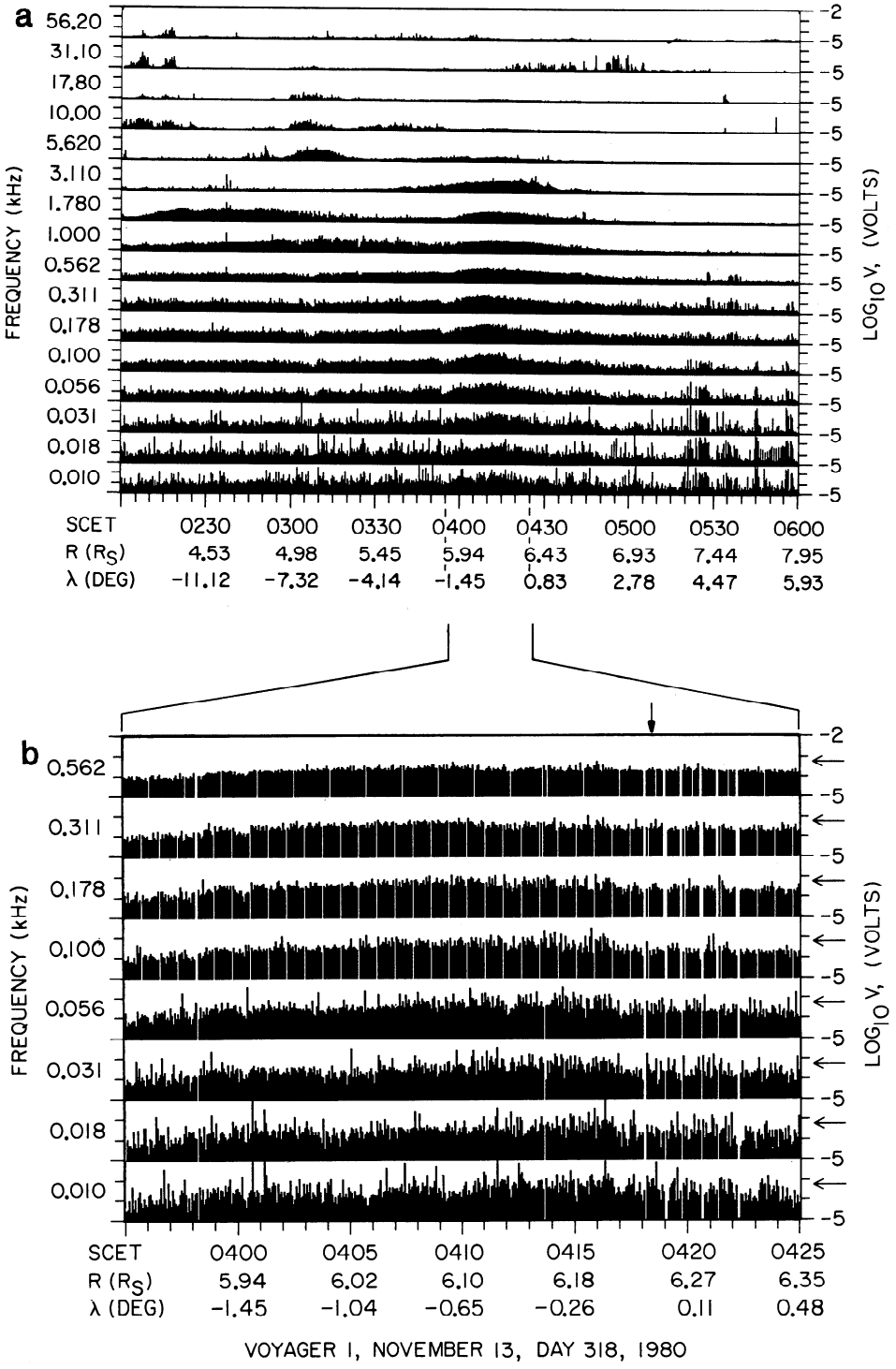

Figure 2. (a) The Voyager 1 plasma wave observations for 4 hours around the equatorial plane crossing. The position of the spacecraft is shown at various SCET's. Note the low-frequency enhancement from about 0400 to 0430 SCET. (b) Voltages of the lowest eight channels of the 16-channel spectrum analyzer near the equatorial plane. Note that the intensity decreases as the frequency increases. The bursty signals superimposed on a smooth background can clearly be seen. The intensity threshold is indicated by an arrow for each channel.

tikidis et al., 1994; *Gurnett et al.*, 1987, 1991]. The similarities are the spiky nature of the bursty signal and the gradual increase and decrease in the broadband intensity (even though the change is slow and the intensity does not reach a very distinct maximum). The fact that the intensity decreases with increasing frequency and drops to the instrument noise level at higher frequencies (above a few kilohertz) is also consistent with what has been recorded by the Voyager 1 and 2 PWS instruments in the various planetary encounters. We attribute the bursty signals to dust impacts.

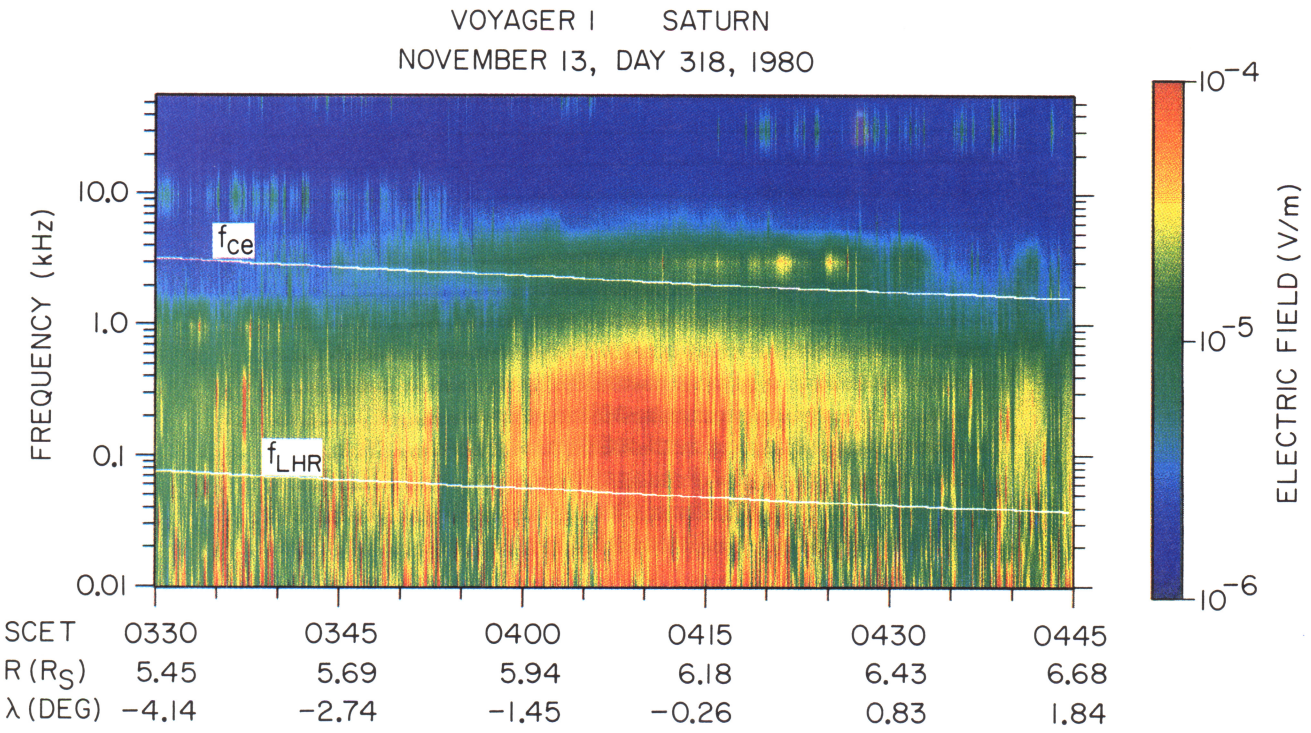

Plate 1. Frequency-time spectrogram for the Voyager 1 encounter with Saturn. Spacecraft event time (SCET) is shown in the abscissa along with the radial distance and latitude of the spacecraft. A false color scheme is utilized where the highest intensities are shown in red and the lowest ones in blue. Superimposed on the spectrogram is the profile of the electron cyclotron frequency $f_{ce} = 28|B|$, where f_{ce} is in units of hertz and B in units of nanoteslas. Also, the lower hybrid resonance frequency f_{LHR} profile can be seen, where $f_{LHR} = (f_{ce}f_{ci})^{1/2}$, f_{ci} being the ion cyclotron frequency. The most intense feature is essentially a magnification (in time) of the feature tentatively labeled as dust in Plate 3 of *Kurth and Gurnett* [1991].

A color spectrogram of the 16-channel spectrum analyzer data taken over a period of time of 1 hour and 15 min is shown in Plate 1, which is similar to Plate 3 of *Kurth and Gurnett* [1991], but with the frequency and timescales changed to illustrate the features of interest. Red indicates the most intense signals, and blue indicates the least intense. The most intense feature ranges in frequency from 10 Hz to 1 kHz, starting slightly before 0400 SCET, and lasting for about 25 min. From now on, we will refer to this feature as the low-frequency equatorial enhancement. The duration of the enhancement above the lower hybrid frequency f_{LHR} is somewhat longer than at lower frequencies. The lower hybrid resonance frequency is defined as $f_{LHR} = (f_{ce}f_{ci})^{1/2}$, where f_{ce} and f_{ci} are the electron and proton cyclotron frequencies, respectively. As mentioned by *Barbosa and Kurth* [1993], waves in the low-frequency equatorial enhancement are good candidates for whistler mode noise since whistler mode emissions propagate below the electron cyclotron frequency. We inspected plasma wave spectra obtained at Earth with the Galileo and other plasma wave instruments. Typically, the whistler mode intensity decreases substantially below the lower hybrid resonance frequency f_{LHR} (see line profile in Plate 1). It should be mentioned that the region sampled by Voyager 1 is probably dominated by O^+ or N^+ [*Bridge et al.*, 1981]. If, for example, the plasma consists of 80% O^+ and 20% protons, then the lower hybrid resonance frequency is reduced by a factor of 2 below the profile provided in Plate 1. Hence minimal plasma wave contamination would be expected in the lowest three channels.

There are several reasons to expect that dust should have been detected by Voyager 1, especially near the equator. *Gurnett et al.* [1983] studied a large number of wideband data frames recorded by both Voyager spacecraft; these indicate the presence of dust throughout the Saturnian system. Even the limited number of Voyager 1 wideband frames, obtained before the equatorial plane crossing, provide a convincing case that dust exists throughout the Saturnian system. At the time that the last Voyager 1 wideband frame was taken at 0326 SCET on November 13, 1980, before the equator crossing (position A in Figure 1), the spacecraft was at a radial distance of 5.38 R_S and latitude of −4.53°. During this frame, numerous dust impact signals were recorded by the wideband receiver. The dust impact signatures are identical to the wideband waveforms observed during the other planetary encounters of Voyager 2. For a full description of these dust impact waveforms, see *Gurnett et al.* [1983, 1987, 1991] and *Tsintikidis et al.* [1994]. Similar waveforms have also been observed during other times when wideband data were available (the day of the year and the times are shown in the first and second columns, respectively, of Table 1) during the Voyager 1 encounter with Saturn. For a complete summary of the Voyager 1 wideband impulse rates, see Table 1 of *Gurnett et al.* [1983]. In addition, from the imaging data we know that Voyager 1 crossed the diffuse E ring [*Smith et al.*, 1981].

Table 1. Various Impact Rates as Derived From the 16-Channel Spectrum Analyzer and the Wideband Waveform Receiver Data at Certain Times (Day of Year and Spacecraft Event Times) Corrected for Numerous Effects

Day of Year	Spacecraft Event Time	Spectrum Analyzer Impact Rate	Impact Rate Corrected for Spacecraft Noise	Wideband Waveform Receiver Impact Rate	Final Impact Rate
317	1001	0.09	0.01	5.36	0.28
317	1257	0.36	0.28	12.06	7.92
317	1830	0.17	0.09	13.57	2.55
317	2107	0.27	0.19	3.53	5.38
318	0109	0.43	0.35	5.72	9.91
318	0326	0.57	0.45	15.87	12.74

Rates are in s^{-1}. The errors associated with the values shown in columns 3, 5 and 6 can be seen in Figures 5 and 6.

Further support for the fact that dust exists in the regions traversed by the Voyager 1 spacecraft can be found in Figure 3, which shows a 1-min average spectrum from 0413 to 0414 SCET, chosen during the time when the low-frequency equatorial enhancement is most prominent. Other 1-min intervals give similar spectra. *Meyer-Vernet et al.* [1986] have shown that a signal dominated by dust impacts has a spectral density which varies as f^{-4}. The f^{-4} spectrum is in agreement with the spectra obtained by the Voyager 2 planetary radio astronomy instrument at Saturn [*Aubier et al.*, 1983] and Uranus [*Meyer-Vernet et al.*, 1986] and to the spectra obtained by the Voyager 2 plasma wave instrument at Saturn [*Tsintikidis et al.*, 1994] and Neptune [*Gurnett et al.*, 1991]. The spectrum of Figure 3 varies approximately as f^{-4}. The slight deviation from the theoretical form is probably due to the presence of plasma wave activity at the same time. The presence of dust impacts in the high-resolution data, the fact that the spacecraft traversed a tenuous ring, and the shape of the spectrum from the low-resolution data all lead us to the conclusion that the Voyager 1 PWS instrument is responding to dust impacts as it crossed the Saturnian equator near 0410 SCET.

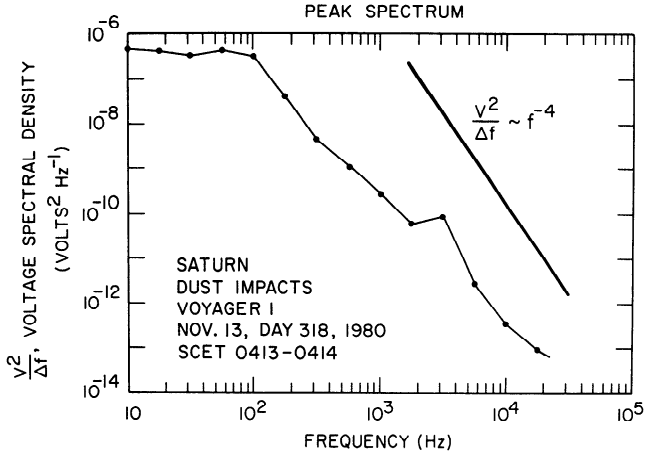

Figure 3. The voltage spectrum during 0413–0414 SCET. The only condition satisfied for choosing this specific time was for the interval to belong to the feature of interest, in other words to the low-frequency equatorial enhancement of Plate 1. The bump at higher frequencies corresponds to the relatively narrow-band feature above the electron cyclotron frequency (electron cyclotron harmonic emission). It can be seen that at frequencies above a few hundred hertz the spectrum variation is between f^{-3} and f^{-4}.

3. Impact Rates and Particle Number Densities

The number density n of the impacting particles is given by

$$R = nUA_{SC}, \tag{1}$$

where R is the impact rate, U is the relative speed between the spacecraft and the particles, and A_{SC} is the effective area of the spacecraft body. The relative speed between the spacecraft and particles in a circular, prograde, equatorial orbit is 29.3 km/s. The effective area is 1.66 m^2 as computed by *Gurnett et al.* [1983]. The greatest difficulty in computing the number density n lies in measuring the impact rate R. Since the 16-channel spectrum analyzer data are the only data available around the time of the equatorial plane crossing, these data must be used to derive impact rates.

Only the lowest eight channels are analyzed to look for impacts, since no bursty signals can be seen in the higher channels. Figure 2b shows the lower eight channels of the spectrum analyzer during the most prominent portion of the low-frequency equatorial enhancement when the smooth background and the bursty signals are more easily seen. Figure 2b is divided into 1-min intervals from 0400 to 0425 SCET. Each burst exceeding a threshold intensity of 7.1×10^{-4} V (indicated by the arrows in Figure 2b) is attributed to a dust impact. This threshold was selected to ensure that the bursts were clearly above the smooth background. Since the 16-channel spectrum analyzer is a step frequency receiver, spikes in different channels cannot be due to simultaneous samples of the same impact.

To obtain an accurate count rate, the duty cycle of the spectrum analyzer must be considered. The instrument effectively samples each channel for 0.05 s, for a total of 0.4 s in all eight channels during the 4-s interval available for an entire spectral sweep. Hence the duty cycle is 0.10. An additional uncertainty involves the number of impacts associated with each peak. The typical timescale of a dust impact as recorded by the wideband receiver is about 10 ms [*Gurnett et al.*, 1983; *Tsintikidis et al.*, 1994]. Each point plotted in Figure 2b represents a ~50 ms measurement period during which any number of dust impacts may have occurred. However, using the maximum impact rate derived from the wideband observations (e.g., ~16 s^{-1} at 0326

Table 2. Calculation of Spurious Event Rates Due to Spacecraft Thruster Firings

Day of Year	Spacecraft Event Time	Duration, min	Thruster Activity Rate, s^{-1}
316	0720	10	0.050
316	1850	15	0.110
316	2301	10	0.083
316	2335	15	0.067

After the times chosen below the thruster activity frequency did not change significantly but the thruster intensity did.

SCET) it is apparent that, on average, there is only about one impact per measuring period. As the rates increase above than 20 s^{-1}, it becomes increasingly likely that two or more impacts can occur within a 50-ms interval, and our assumption of 1 impact per peak becomes a lower limit. There is no way of telling the number of impacts solely from the spectrum analyzer data. Throughout this study it will be assumed that each burst corresponds to a single dust impact. This assumption will be further justified shortly.

After each planetary encounter the spectrum analyzer data were processed to remove unwanted data in the following sense: periodic bursty signals that were clearly due to instrument interference (e.g., due to the stepper motor in the low-energy charged particles instrument) were removed from the data set. The effects of this processing can be seen by the periodic gaps in Figure 2b. Hence the contribution of the aforementioned interference was close to zero for the signal under study. However, some aperiodic spacecraft-related interference signals also occurred. The primary source of these unpredictable interference signals in the lower eight channels was random attitude control thruster activity. There were no data from the spacecraft that indicated exactly when the thruster firings occurred. However, it was necessary to correct the impact rates by taking the contribution of the thruster activity into account.

To correct for thruster interference effects, various times were considered during which the spacecraft was far from the planet (out in the solar wind) where dust impacts are highly unlikely. Outside of the Saturnian system, it can be assumed that the only significant source of low-frequency bursts is thruster activity. For these periods the spurious event rates exceeding the threshold are calculated and corrected for the duty cycle. To first order, encounter-related spacecraft activities near the equator crossing were similar to these control intervals, so thruster activity would also be expected to be similar. The results can be seen in Table 2. The average spurious event rate was found to be 0.08 s^{-1}. This value was subtracted from the impact rate determined closer to the planet (column 4 in Table 1).

While the spacecraft was close to the planet and before it crossed the equatorial plane, there were six intervals during which 48-s wideband waveform data frames were taken. At these six intervals the impact rates were found by visually inspecting the waveforms (column 5 in Table 1). The highest impact rate occurred at 0326 SCET and was 15.87 s^{-1}. The probability of having a second impact during a 50-ms measurement was very low, approximately 0.6%. Hence the assumption that there is only one impact per 50-ms peak is justified for all measurement periods. There is a slight difference between the newly derived impact rates and the ones listed in Table 1 of *Gurnett et al.* [1983]. In general, the new impact rates are higher than the older ones. The difference is attributed to the fact that in this study the impact rates were determined by visual inspection and actual count of events, whereas in the study of *Gurnett et al.* [1983] the rates were determined by listening for individual impacts on an audio recording of the waveforms. During the same six intervals, and for 5-min intervals centered at the times of the wideband data recordings, the impact rates from the 16-channel spectrum analyzer data were found by counting the number of peaks that exceeded the amplitude threshold and correcting for the duty cycle and spacecraft interference. It was assumed that the impact rate does not change significantly over a few minutes.

Next, the corrected impact rates from the 16-channel spectrum analyzer data and from the wideband waveform data were compared. There is a difference between the former and the latter due to the different sensitivities of the two methods. The spectrum analyzer rates are lower than those determined using the waveforms since the wideband receiver is more sensitive to dust impacts than the spectrum analyzer. This increased sensitivity to dust impacts arises because the distinctive nature of the impact waveform allows a very reliable count of even very small amplitude impacts. To assure that we are only using bursty events (dust impacts) in the spectrum analyzer data, we had to use quite large amplitude thresholds.

The difference between the impact rates derived by the two methods can be explained with the aid of Figure 4, which shows a hypothetical distribution of the number of impacts with impact "amplitude." The impact amplitude is a function of dust mass, dust and target composition, relative speed, and impact geometry. If the PWS instrument was able to detect all possible particles, then the number of impacts would be given by the entire area under the curve in Figure 4. However, the waveform receiver subsystem detects only impacts above its threshold as indicated by the hatched area

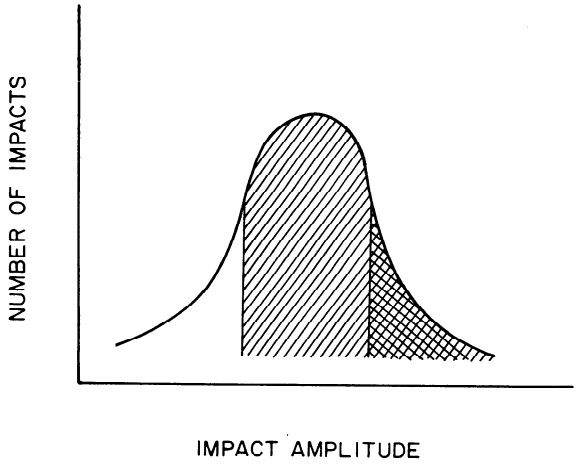

Figure 4. A hypothetical distribution of the number of impacts with impact amplitude. Impact amplitude denotes the intensity of the signal and depends on the particle mass, composition, speed, and impact geometry. The hatched area indicates the number of impacts that the waveform receiver detects that are above its threshold. The cross-hatched area corresponds to the number of impacts that produce signals that are above the spectrum analyzer's threshold.

in Figure 4. Since the spectrum analyzer method has a lower sensitivity, hence higher threshold as described above, this method detects an even smaller fraction of the total distribution (cross-hatched area in Figure 4). Therefore, for a reasonably regular distribution function the difference between impact rates from the two methods should be the difference of the hatched and cross-hatched areas in Figure 4. This provides the rationale for scaling the spectrum analyzer rates described below. The next logical step is to calculate the average correction factor between the impact rates determined by the two methods. This way, the impact rates derived from the wideband waveform data can be used to calibrate the spectrum analyzer rates. The average correction factor was calculated to be approximately 30 and the spectrum analyzer impact rates were multiplied by this factor. Figure 5 shows the agreement between the two impact rates after multiplying the rates derived from the spectrum analyzer by the correction factor. Excluding the first and third points, one can see that the agreement between the rest of the points is quite good. The first and third point discrepancies were not included in the calculation of the average correction factor because of gaps in the low rate data during the 5-min intervals that correspond to the first and third wideband samples.

It is important to consider the response of the spectrum analyzer to short-duration signals since the time constant is a function of frequency. The response of the spectrum analyzer is subject to the constraint $\Delta f \Delta t \simeq 1$, where Δf is the filter bandwidth and Δt is the duration of the signal. As the channel frequency decreases, Δf decreases and Δt increases since the bandwidth of the filters are $\sim \pm 15\%$ of the center frequency. A signal sampled at, say 10 Hz, takes about one second to decay. Hence this channel is effectively "active" for much longer than the 50-ms time constant of the log compressor discussed above, and the effective duty cycle is greater than 0.1. At higher frequencies the filter bandwidth is larger (e.g., about 100 Hz for the 562-Hz channel), and the channel time constant is set by the 50-ms time constant of the log compressor. Therefore, at high frequencies, above about 500 Hz, short duration (~10 ms) pulses are underestimated or missed completely, especially if they occur early in the 50-ms measurement period. Hence the duty cycle in the 562-Hz channel is substantially less than assumed above. This is one of the main reasons that in the lowest four channels of Figure 2b a large number of bursts were detected that exceeded the preset threshold and that substantially fewer bursts exceed the preset threshold in the upper 4 channels of Figure 2b. By calibrating the spectrum analyzer impact rates with the waveform receiver impact rates (as shown in Figure 5) we compensate for any errors that the varying time constant might have introduced.

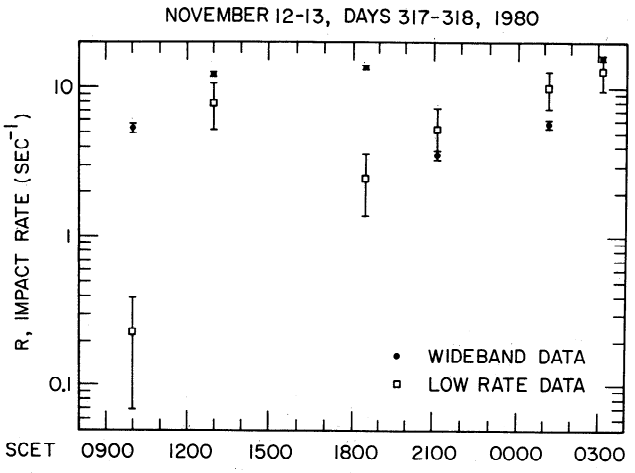

Figure 5. A comparison of the impact rates as deduced from the wideband data and the 16-channel spectrum analyzer data. The latter has already been multiplied by the average discrepancy factor of 28.3. The error bars are 1 σ.

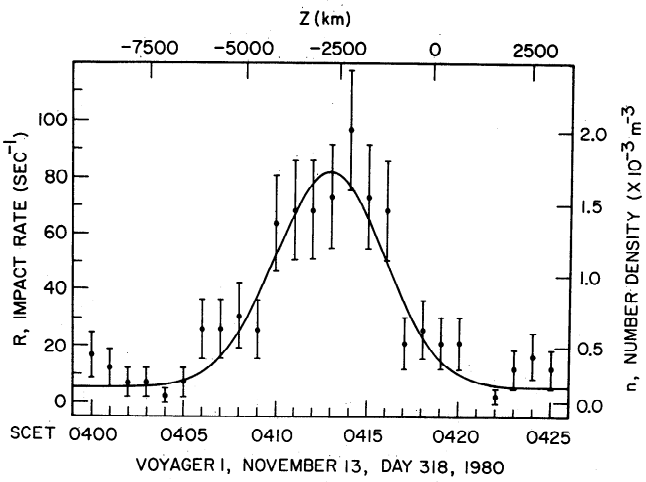

Figure 6. The impact rate profile obtained from the 16-channel spectrum analyzer data. Note the clear peak centered about 2500 km below the equatorial plane crossing by the spacecraft. The error bars are 1 σ.

The average ratio of impact rates determined by dividing the wideband waveform receiver data by the 16-channel spectrum analyzer data was used to multiply the impact rates from the 16-channel spectrum analyzer during the interval from 0400 to 0425 SCET around the equatorial plane crossing of the spacecraft. The results are shown in Figure 6. A well-defined peak can be seen when the spacecraft was about 2500 km below the equatorial plane. If one assumes that the particle distribution depends only on the distance z from the equatorial plane, a Gaussian profile can be used to fit the impact rate profile. A good fit is given by a function of the form

$$R = R_0 + R_1 \exp\left[\frac{-(z-h)^2}{\Delta z^2}\right], \qquad (2)$$

where h is the offset of the symmetry axis from the equatorial plane and Δz is the thickness of the Gaussian component. The best fit values are $R_0 = 5(\pm 1)\ s^{-1}$, $R_1 = 76(\pm 9)\ s^{-1}$, $h = -2470(\pm 150)$ km, and $\Delta z = 2065(\pm 225)$ km. This fit is shown as a solid line in Figure 6. Having obtained the impact rate profile, it is easy to return to (1) and derive the number density profile. The results can also be seen in Figure 6 (right scale). The peak number density is a little over 0.002 m^{-3} and occurs when the spacecraft is about 2500 km south of the equatorial plane.

4. Antenna Voltages and Grain Masses

When a small particle hits a solid surface at a velocity of a few kilometers per second or greater, the particle and some

of the surface material are instantly vaporized and heated to a high temperature $\sim 10^5$ °K [*Gurnett et al.*, 1991]. At these high temperatures a portion of the gas is ionized, thereby producing a plasma cloud that expands rapidly outward from the impact site. Results of laboratory experiments [*Grün*, 1981] show that the charge Q released at the impact site is proportional to the mass m of the impacting particle,

$$Q = km, \tag{3}$$

where k is a yield coefficient that depends on the velocity of the particle and the composition of the particle and the target. During the time interval that the low-frequency equatorial enhancement was recorded, the relative speed between the spacecraft and particles in prograde, circular orbits was very high, approximately 29.3 km/s. Using the fact that laboratory experiments indicate that the yield coefficient varies approximately as the cube of the speed [*Grün*, 1981], we calculated the yield constant to be 2.05 C/g.

The basic assumption in our study is that only a fraction α of the charge released after the impact is collected by the antennas, hence producing a voltage pulse of amplitude:

$$V = \alpha(Q/C_A), \tag{4}$$

where C_A is the antenna capacity. The constant α is the effective charge collection coefficient. The coefficient is dimensionless and was estimated by *Tsintikidis et al.* [1994] to be 0.0078. The coefficient is an average value and was calculated by using the Voyager 2 planetary radio astronomy instrument (PRA) to calibrate the PWS instrument at all available ring plane crossings, namely at Saturn, Uranus, and Neptune (both inbound and outbound for the latter). The implicit assumption is that the same value of α that was calculated based on Voyager 2 data can be used for Voyager 1 since both spacecraft have identical PWS and PRA instruments. For more details on the calculation of α, see *Tsintikidis et al.* [1994].

As mentioned in the previous chapter the threshold intensity for detecting dust impacts was set at 7.1×10^{-4} V. The actual mass detection threshold for the wideband waveform receiver is smaller than given above because the waveform receiver has a higher sensitivity, hence lower threshold, than the 16-channel spectrum analyzer, a fact that was also shown in Figure 4.

It is useful to find the equivalent mass detection threshold for the waveform receiver since the impact rate detected from the spectrum analyzer data was calibrated with impact rates derived from the wideband waveform receiver. This threshold can be used as a lower limit for the derivation of particle sizes. The $V_{\rm rms}$ voltage profile (over time) was calculated for a few minutes around 0326 SCET. The frame at 0326 SCET is the last time that wideband waveforms were recorded before Voyager 1 crossed the equatorial plane. The $V_{\rm rms}$ profile around this time is shown in Figure 7. The lowest $V_{\rm rms}$ value at 0326 SCET was considered to be the voltage that corresponds to the waveform receiver mass detection threshold m^*, since any larger impacting particle would exceed this voltage threshold. The lowest rms voltage was found to be approximately 5.0×10^{-4} V and is shown by an arrow in Figure 7. Next, the following equation was used to calculate m^*,

$$m* = (\beta C_A/\alpha k)V_{\rm rms}. \tag{5}$$

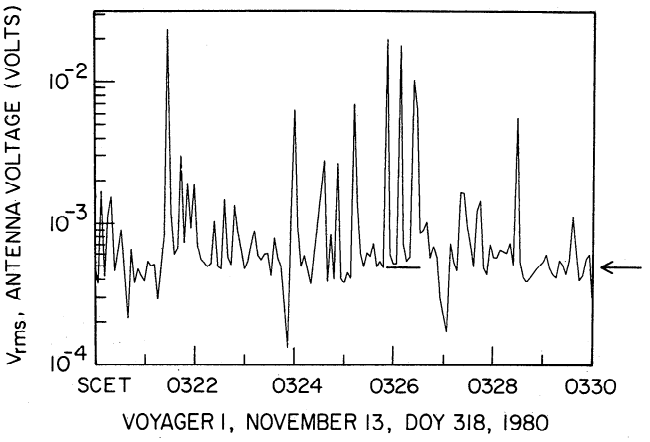

Figure 7. The rms voltage profile obtained around 0326 SCET. At that time the last wideband data frame was taken. The arrow indicates the waveform receiver voltage (5.0×10^{-4} V) corresponding to a mass detection threshold of 1.4×10^{-12} g. This corresponds to an icy particle that has a radius of 0.7 μm.

Equation (5) was first used by *Gurnett et al.* [1983]. The instrument-related constant β is dimensionless and $\beta = 0.51$, $C_A = 90$ pF is the antenna capacity [*Gurnett et al.*, 1983], $k = 2.05$ C/g, and $\alpha = 0.0078$. Hence m^* was found to be 1.4×10^{-12} g, which corresponds to an icy particle of 0.7 μm in radius. In essence the Voyager 1 wideband waveform receiver would be able to detect particles that are about 0.7 μm in radius or larger had it been used during the Voyager 1 equatorial crossing of Saturn. Since the spectrum analyzer rates were calibrated with the waveform data, this is also the effective size threshold for the spectrum analyzer-determined rates. It was shown by *Gurnett et al.* [1987] that the rms mass of the particles that impacted the Voyager 2 spacecraft during the Saturnian ring plane crossing is given by

$$m_{\rm rms} = (C_A/\alpha k)[1/(R\tau)^{1/2}]V_{\rm rms}. \tag{6}$$

R is the impact rate and τ is the duration of a typical, unclipped pulse. Equation (6) will be used in the Voyager 1 case. As can be seen in (6), the $V_{\rm rms}$ voltage value is necessary in order to calculate the masses.

The rms voltage for the PWS measurements is obtained by integrating the voltage spectrum over frequency. Hence each individual frequency (or channel) contributes to the total $V_{\rm rms}$. The contribution to each channel is given by the ratio $V_i/V_{\rm rms}$, where V_i is the voltage recorded by the ith channel. In general, the total $V_{\rm rms}$ voltage varies for different ring plane crossings. However, the contribution of each channel to the total rms voltage remains the same as long as the shape of the spectrum is the same. In other words, if $V_{\rm rms}$ is reduced, V_i is also reduced in such a manner as to keep the aforementioned ratio constant. The $V_{\rm rms}^{\rm V2}$ voltage recorded by Voyager 2 during the Saturnian ring plane crossing reached a maximum value of 0.137 V. A typical peak voltage value V_i was obtained with the aid of Figure 8 for each of the lowest four channels (hence $i = 1$ to 4) during the crossing. In other words, the top four leftmost crosses in Figure 8 were used since the peaks were more pronounced in these channels. Also, because of the longer response of the

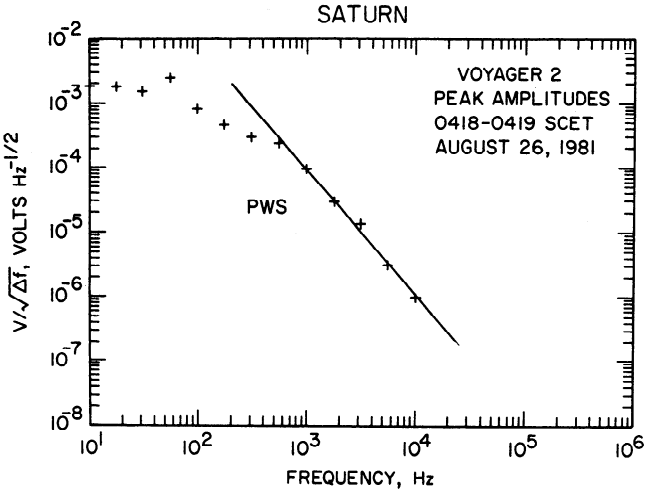

Figure 8. This figure is adapted from Figure 7a of *Tsintikidis et al.* [1994]. The time interval corresponds to the Voyager 2 crossing of the Saturnian ring plane and V_{rms} = 0.137 V.

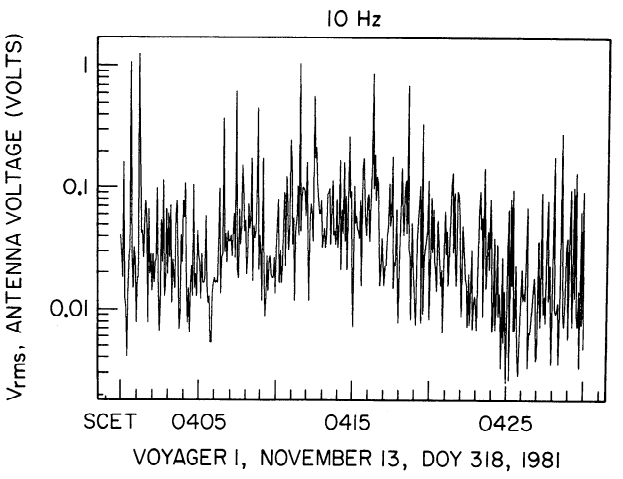

Figure 9. The V_{rms} profile for Voyager 1 obtained with the aid of the V_{rms} profile of Voyager 2. The Voyager 1 profile was obtained for the first channel (10.0 Hz). Similar profiles in shapes and intensities were obtained for channels 2 and 3 (17.8 and 31.1 Hz, respectively).

narrowband filter, the instrument can more accurately measure the amplitude of short duration impulses. Next the ratios V_{rms}^{V2}/V_i were computed (see column 2 in Table 3). In essence the ratios show the inverse of the contribution to the total rms voltage profile from each frequency channel. Since the instrumentation and impact physics are identical, it is expected that V_{rms}^{V1}/V_i ratio would be equal to the Voyager 2 V_{rms}^{V2}/V_i ratio. Hence the following equality can be obtained:

$$V_{rms}^{V2}/V_i^{V2} = V_{rms}^{V1}/V_i^{V1}. \quad (7)$$

The V_i^{V1} values can be taken to be the values of the bursts that exceeded the preset threshold indicated by the arrows in Figure 2b. The only unknown in (7) is V_{rms}^{V1}. Hence, solving (7) for V_{rms}^{V1}, an estimate of the rms voltage can be obtained for Voyager 1. Four V_{rms}^{V1} values resulting from V_i^{V1} values for four typical bursts are shown in Table 3. The average rms voltage is about 0.07 V. For this value the rms mass is 1.2×10^{-9} g from (6). The peak impact rate used in (6) was $R = 96$ s^{-1} and the value $\tau = 1$ ms was used for the duration of the pulse. Hence the mass corresponds to a 6.5-μm icy particle with $\rho = 1$ g/cm^3 or to a 5.2-μm silicate particle with $\rho = 2$ g/cm^3.

The spikes in the spectrum analyzer data correspond to particles that are in the far right wing of the hypothetical distribution of Figure 4. If one considers the uncertainties pertaining to the geometry of the impact, or target material (e.g., gold has a yield constant that is 6 times larger than the yield constant of aluminum [*Grün*, 1981]), or the impact velocity, then it is likely that the actual particle radii are less than 5 μm. Unfortunately, there is no way of obtaining more precise results from the 16-channel spectrum analyzer data. It should be emphasized that the particle radii determined with the above method are at best rough estimates.

One can use the above method to derive a V_{rms} profile using the first channel (10 Hz) for the Voyager 1 case. In the above discussion, we concentrated on the spikes in this profile. We also concluded that the larger amplitudes may be due to effects other than large dust particles. Now we will analyze the background "continuum," assuming that it is at least partially due to dust impacts. The background voltage profile can be seen in Figure 9. This way we are concentrating more on the bulk of the particle distribution. Since the background is of primary interest, large fluctuations can be ignored. The background level is seen to be about 0.03 V, which using (6) gives $m_{rms} = 5.3 \times 10^{-10}$ g. This value corresponds to a 5.0-μm icy particle or to a 4.0-μm silicate particle. It seems that the Voyager 1 spectrum analyzer is detecting particles that are up to a few microns in radius. The above value should be regarded as an upper limit because it is certain that plasma wave activity provides some contribution to the total V_{rms}. Furthermore, as was discussed earlier, the time constant in the lowest channel is much larger than 50 ms. Because of the long time constant and the fact that we have almost 16 impacts per second, it is possible that some bursts may have resulted from a pile-up effect. Hence the computed mass could be the cumulative mass due to multiple impacts. Similar profiles to the one shown in Figure 9 were obtained for the second and third channels (17.8 and 31.1 Hz, respectively).

Table 3. Calculation for the Voyager 1 V_{rms} Values at the Lowest Four Frequencies

Frequency, Hz	V_{rms}^{V2}/V_i^{V2}	V_i^{V1}, V	V_{rms}^{V1}, V
10.0	40.48	2.1×10^{-3}	0.085
17.8	39.96	1.0×10^{-3}	0.040
31.1	41.80	9.0×10^{-4}	0.038
56.2	29.92	4.0×10^{-3}	0.120

5. Discussion

A study has been performed of the impulsive noise that the plasma wave instrument detected near the equatorial plane during the Voyager 1 flyby of Saturn. It has been shown that this noise can be attributed in part to dust particle impacts. The mass threshold for detecting these particles is 1.4×10^{-12} g. The size of the particles is estimated to be a few microns. The particle impacts were detected when the

spacecraft was in the vicinity of the equatorial plane and the impact rate peaked when the spacecraft was 2470 (±150) km south of the plane. The north-south thickness of the impact region is 4130(±450) km FWHM (full-width, half-maximum) based on a Gaussian fit. At the maximum impact rate the maximum number density of the particles was derived to be about 10^{-3} m^{-3}, which corresponds to interparticle distances on the order of 10 m. The picture that emerges is of a 4000-km-thick "disk" of micron-sized particles located 2500 km south of the equatorial plane. The low impact rates that correspond to the Gaussian wings of Figure 4 and the impact rates derived from the wideband receiver indicate that there is also a broader region with lower dust densities or background "halo."

The properties of Saturnian dust particles have been studied before by *Gurnett et al.* [1983] and *Tsintikidis et al.* [1994] using the PWS instrument data. The difference between the method used in this study and the method used in the previous studies lies in how the impact rate profile and the mass values are derived. In the previous studies the wideband waveform receiver data were used to measure impact rates. In this study the 16-channel spectrum analyzer data had to be used, since no high-resolution data were available during the equator plane crossing. However, the few high-resolution data frames available at other times were still of use in order to calibrate the low-resolution results. The current method could not have been used by, for example, *Gurnett et al.* [1991], due to the uncertainty in the number of impacts responsible for each spike (see, for example, their Figure 2) since the very large impact rates imply multiple impacts within a 50-ms measurement interval. The same situation also occurs for the other planetary ring plane crossings by Voyager 2. It was fortunate that Voyager 1 crossed the E ring region at a high speed and in a region of the ring with a relatively low density. The large relative speed between the particles and the spacecraft resulted in more charge (as opposed to less charge being released at small relative speed) being released during a dust impact (k = 2.05 C/g), hence enabling the plasma wave instrument to detect the impact. The low number densities resulted in the spikes being well separated from each other. The above two factors allowed the spikes to be distinguished from the background plasma wave activity.

The particle masses in the present study were derived with the aid of the $V_{\rm rms}$ profile obtained during the Voyager 2 crossing of the Saturnian ring plane. In the present case the signal recorded by the PWS instrument is due to a combination of dust impacts noise and plasma wave signals. Furthermore, for this reason the mass estimate should be regarded as an upper limit.

It is useful to compare our findings with those of other studies. *Showalter et al.* [1991] performed an extensive analysis of a set of photometric data of Saturn's E ring. They concluded that the ring consists of slightly nonspherical particles whose size distribution is narrow: 1.0(±0.3) μm. This size is comparable to, but smaller than, the sizes obtained in this study. Since the $V_{\rm rms}$ profile (Figure 7) does not vary smoothly as was the case in the Voyager 2 ring plane crossings of the outer planets, we cannot really deduce any information about the particle size distribution. An attempt to permit the particles to be about 1 μm in radius resulted in the following: the product αk that appears in (6) will have to become larger than its current value by about 2 orders of magnitude, a fact that contradicts results from laboratory experiments, or $V_{\rm rms}$ should be smaller by about 2 orders of magnitude bringing the voltage values under the detection threshold. On the other hand, we have better agreement with *Randall* [1994]. Using the absorption signature of energetic electrons in Saturn's magnetosphere, *Randall* [1994] concluded that the E ring particle radii are in the range of 0.4 to 3.2 μm.

One can use the best fit Gaussian profiles or, equivalently, the number density profiles to derive the columnar number density perpendicular to the equator plane. The columnar number density is $\kappa = \pi(n_1 \Delta z_1)$ and $\kappa = 2.0(\pm 0.6) \times 10^4$ particles/m^2. The quantity n_1 is the number density that corresponds to R_1 of (2). The quantity Δz_1 is the width of the Gaussian derived from (2). The R_0 term has been ignored since it is smaller than R_1, and there is no way of calculating the thickness associated with it. From the columnar number density and the particle size the optical depth can be derived. The optical depth τ is a measure of the fraction of the area covered by particles along the column perpendicular to the ecliptic plane. If a typical radius of 4 μm is used, then the particle cross-sectional area is $A_0 = 5.0 \times 10^{-11}$ m^2. The optical depth becomes $\tau = A_0 \kappa = 1.0(\pm 0.3) \times 10^{-6}$. However, it should be kept in mind that the optical depth is underestimated because it does not include particles below the instrument counting threshold. For the location traversed by Voyager 1 the optical depth normal to the equatorial plane as given by the photometric study of *Showalter et al.* [1991] is about 4.0×10^{-7}, smaller than the optical depth calculated in the present study by a factor of about 3. Several reasons may account for the difference. The Voyager 1 cameras cover a large area (global technique), whereas the PWS instrument detected only the particles along the trajectory of the spacecraft and which were above a well-defined sensitivity threshold (local technique). The yield constant k comes from an empirical rule [*Grün*, 1981]. The k value for water is not known so it had to be estimated from other materials and it could be off by a factor of 3 or more [*Gurnett et al.*, 1983]. The impact geometry and impact site on the spacecraft are also not well known. Of course, it should be kept in mind that plasma wave activity is masking some of the dust impact noise, which would further decrease the estimated mass.

It is widely accepted that Enceladus is the primary source of the E ring's micron-sized dust particles [*Showalter et al.*, 1991; *Horanyi et al.*, 1992; *Hamilton*, 1993]. The moon is located at 3.95 R_s, and its surface is very smooth. The smoothness of the surface indicates that the moon was geologically active in the distant past, either through volcanism [*Pang et al.*, 1984] or geyserlike eruptions [*Haff et al.*, 1983]. Observations show that the thickness of the E ring at its outer edge is about 40,000 km [*Showalter et al.*, 1991]. The dynamics of E ring particles, from computer simulations, favors a northward asymmetry rather than the southward asymmetry presented herein (D. Hamilton, personal communication, 1993). The simulation asymmetry is a result of the quadrupole component of the Saturnian magnetic field. The dust detected by the Voyager 1 PWS is concentrated predominantly south of the equatorial plane. Also, in order to be able to align our observations with the equatorial plane, the spacecraft should have recorded the impacts at least 5 to 7 min after it really did. There is no way in which we can rationalize such a large error in timing. The vertical

extent of the micron-sized dust particles in the model used by *Hamilton* [1993] barely reaches the north part of the dust cloud derived from our study. Our observation model can account for the existence of a few micron-sized dust particles up to about 2500 km north of the equatorial plane (right wing of the Gaussian profile in Figure 6).

Recently, *Hamilton and Burns* [1994] proposed that the *E* ring may be self-sustained. Enceladus, located at a strategic location within the *E* ring, acts as a sink that can in fact erode the ring in about 20 years. Hence there has to exist a source for dust. The Hamilton-Burns mechanism is provided by the particle-Moon collisions. According to their theory, dust particles can strike a Moon, that is, in a low eccentricity orbit. The authors show that micron-sized particles can become very energetic (i.e., velocities of about 10 km/s) mainly due to the large eccentricities that they can attain. As these particles hit a moon, they produce ejecta that escape into orbits around the planet. The mass of the ejecta can be equal to or larger than the mass of the original particles. It was shown by the aforementioned authors that only the micron-sized particles can become members of the *E* ring. The larger particles are short-lived and reside near the Moon's orbit before eventually falling back to the moon in low-energy collisions that free up little or no mass at all. It is possible that this same mechanism is responsible for ejecting particles from Dione. The spacecraft was very close to Dione's orbit, and it may have intercepted a localized ringlet which is not characteristic of the overall *E* ring. Furthermore, the Hamilton-Burns mechanism can account for the larger than one micron particles we observe. The mechanism, however, cannot account for the southward offset derived in our study.

A comparison of the PWS and PRA results is now appropriate. *Aubier et al.* [1983] attributed the noise that the Voyager 1 PRA instrument detected during the equator plane crossing to shot noise. Shot noise is due to electrons hitting the spacecraft antennas. The power spectrum of shot noise varies as f^{-2} and is smooth, and broadband (A. Keller, private communication, 1993). However, the Voyager 1 PWS observations at Saturn did not have these characteristics. It can be seen from Figure 2b that the PWS noise exhibits bursts that are inconsistent with the smooth nature of shot noise. Also, the observed power spectrum does not exhibit the f^{-2} behavior expected from shot noise. In fact, the slope of the spectrum obtained by connecting the PWS and PRA measurements in Figure 1 of *Aubier et al.* [1983] is closer to f^{-4} (associated with dust impacts) than to the f^{-2} fit shown in their figure, relying primarily on the high-frequency PRA data. Given the present analysis, we conclude that the observations are more consistent with dust impacts than shot noise.

In view of the Hamilton-Burns mechanism and the results of the present study, a new role may be assigned to Dione as a source of dust particles and its connection with the *E* ring in general. More light will be shed on Dione's role when the Cassini spacecraft visits Saturn and its moons.

Acknowledgments. The authors wish to acknowledge very stimulating discussions with Doug Hamilton, Larry Molnar, and Dave Dunn. We wish to thank Larry Granroth and Scott Allendorf for the valuable advice they gave on computer matters. Useful discussions with Andy Keller and Mihaly Horanyi are also acknowledged; and last but not least we would like to thank Kathy Kurth for taking care of the appearance of the manuscript. This work was supported by contract 959193 with the Jet Propulsion Laboratory.

The Editor thanks J. N. Cuzzi, J. A. Burns, and another referee for their assistance in evaluating this paper.

References

Aubier, M. G., N. Meyer-Vernet, and B. M. Pedersen, Shot noise from grain and particle impacts in Saturn's ring plane, *Geophys. Res. Lett.*, *10*, 5, 1983.

Barbosa, D. D., and W. S. Kurth, On the generation of plasma waves in Saturn's inner magnetosphere, *J. Geophys. Res.*, *98*, 9351, 1993.

Bridge, H. S., et al., Plasma observations near Saturn: Initial results from Voyager 1, *Science*, *212*, 217, 1981.

Burns, J. A., and L. Shaffer, Orbital evolution of circumplanetary dust by resonant charge variations, *Nature*, *337*, 340, 1989.

Grün, E., Experimental studies of impact ionization, *Eur. Space Agency Spec. Publ., ESA SP-155*, Paris, 1981.

Gurnett, D. A., E. Grün, D. Gallagher, W. S. Kurth, and F. L. Scarf, Micron sized particles detected near Saturn by the Voyager plasma wave instrument, *Icarus*, *53*, 236, 1983.

Gurnett, D. A., W. S. Kurth, F. L. Scarf, J. A. Burns, J. N. Cuzzi, and E. Grün, Micron-sized particles detected near Uranus by the Voyager plasma wave instrument, *J. Geophys. Res.*, *92*, 14,959, 1987.

Gurnett, D. A., W. S. Kurth, L. J. Granroth, S. C. Allendorf, and R. L. Poynter, Micron-sized particles detected near Neptune by the Voyager plasma wave instrument, *J. Geophys. Res.*, *96*, 19,177, 1991.

Haff, P. K., A. Eviatar, and G. L. Siscoe, Ring and plasma: The enigmas of Enceladus, *Icarus*, *56*, 426, 1983.

Hamilton, D. P., Motion of dust in a planetary magnetosphere: Orbit-averaged equations for oblateness, electromagnetic, and radiation forces with application to Saturn's E ring, *Icarus*, *101*, 244, 1993.

Hamilton, D. P., and J. A. Burns, Origin of Saturn's E ring: Self sustained, naturally, *Science*, *264*, 550, 1994.

Horanyi, M., J. A. Burns, and D. P. Hamilton, The dynamics of the Saturn E ring particles, *Icarus*, *97*, 248, 1992.

Humes, D. H., Results of Pioneer 10 and 11 meteoroid experiments: Interplanetary and near-Saturn, *J. Geophys. Res.*, *85*, 5841, 1980.

Kurth, W. S., and D. A. Gurnett, Plasma waves in planetary magnetospheres, *J. Geophys. Res.*, *96*, 18,977, 1991.

Kurth, W. S., D. A. Gurnett, and F. L. Scarf, A search for Saturn electrostatic discharges in the Voyager plasma wave data, *Icarus*, *53*, 255, 1983.

Meyer-Vernet, N., M. G. Aubier, and B. M. Pedersen, Voyager 2 at Uranus: Grain impacts in the ring plane, *Geophys. Res. Lett.*, *13*, 617, 1986.

Pang, K. D., C. C. Voge, J. W. Rhoads, and J. M. Ajello, The E ring of Saturn and satellite Enceladus, *J. Geophys. Res.*, *89*, 9459, 1984.

Pedersen, B. M., N. Meyer-Vernet, M. G. Aubier, and P. Zarka, Dust distribution around Neptune: Grain impacts near the ring plane measured by the Voyager planetary radio astronomy experiment, *J. Geophys. Res.*, *96*, 19,187, 1991.

Randall, B. A., Energetic electrons in the magnetosphere of Saturn, *J. Geophys. Res.*, *99*, 8771, 1994.

Scarf, F. L., and D. A. Gurnett, A plasma wave investigation for the Voyager mission, *Space Sci. Rev.*, *21*, 289, 1977.

Scarf, F. L., D. A. Gurnett, W. S. Kurth, and R. L. Poynter, Voyager 2 plasma wave observations at Saturn, *Science*, *215*, 287, 1982.

Showalter, M. R., J. N. Cuzzi, and S. M. Larson, Structure and particle properties of Saturn's E ring, *Icarus*, *94*, 451, 1991.

Smith, B. A., et al., Encounter with Saturn: Voyager 1 imaging science results, *Science*, *212*, 163, 1981.

Tsintikidis, D., D. A. Gurnett, L. J. Granroth, S. C. Allendorf, and W. S. Kurth, Revised analysis of micron-sized particles near Saturn by the Voyager 2 plasma wave instrument, *J. Geophys. Res.*, *99*, 2261, 1994.

Warwick, J. W., D. R. Evans, J. H. Romig, J. K. Alexander, M. D. Desch, M. L. Kaiser, M. Aubier, Y. Leblanc, A. Lecacheux, and B. M. Pedersen, Planetary radio astronomy observations from Voyager 2 near Saturn, *Science*, *215*, 582, 1982.

Xu, R.-L., and H. L. F. Houpis, The stability of the oscillation motion of charged grains in the Saturnian ring system, *J. Geophys. Res.*, *90*, 1375, 1985.

D. D. Barbosa, Institute of Geophysics and Planetary Physics, University of California, Los Angeles, CA 90024.

D. A. Gurnett, W. S. Kurth, and D. Tsintikidis, Department of Physics and Astronomy, University of Iowa, Iowa City, IA 52242.

(Received August 20, 1993; revised August 31, 1994; accepted September 6, 1994.)